Cell. Mol. Life Sci. (2011) 68:1455–1466
DOI 10.1007/s00018-010-0533-1

Cellular and Molecular Life Sciences

RESEARCH ARTICLE

Poly(ADP-ribose)glycohydrolase is an upstream regulator of Ca^{2+} fluxes in oxidative cell death

C. Blenn · P. Wyrsch · J. Bader · M. Bollhalder · Felix R. Althaus

Received: 30 June 2010 / Revised: 18 August 2010 / Accepted: 7 September 2010 / Published online: 29 September 2010

Abstract Oxidative DNA damage to cells activates poly(ADP-ribose)polymerase-1 (PARP-1) and the poly (ADP-ribose) formed is rapidly degraded to ADP-ribose by poly(ADP-ribose)glycohydrolase (PARG). Here we show that PARP-1 and PARG control extracellular Ca^{2+} fluxes through melastatin-like transient receptor potential 2 channels (TRPM2) in a cell death signaling pathway. TRPM2 activation accounts for essentially the entire Ca^{2+} influx into the cytosol, activating caspases and causing the translocation of apoptosis inducing factor (AIF) from the inner mitochondrial membrane to the nucleus followed by cell death. Abrogation of PARP-1 or PARG function disrupts these signals and reduces cell death. ADP-ribose-loading of cells induces Ca^{2+} fluxes in the absence of oxidative damage, suggesting that ADP-ribose is the key metabolite of the PARP-1/PARG system regulating TRPM2. We conclude that PARP-1/PARG control a cell death signal pathway that operates between five different cell compartments and communicates via three types of chemical messengers: a nucleotide, a cation, and proteins.

Keywords ADP-ribose · Poly(ADP-ribose) · H_2O_2 · PARP · PARG · AIF · TRPM2 · Calcium

C. Blenn and P. Wyrsch contributed equally to this work.

Electronic supplementary material The online version of this article (doi:10.1007/s00018-010-0533-1) contains supplementary material, which is available to authorized users.

C. Blenn · P. Wyrsch · J. Bader · M. Bollhalder · F. R. Althaus (✉)
Institute of Pharmacology and Toxicology,
University of Zurich-Vetsuisse,
Winterthurerstrasse 260, 8057 Zurich, Switzerland
e-mail: fra@vetpharm.uzh.ch

Abbreviations

AIF	Apoptosis-inducing factor
PAR	Poly(ADP-ribose)
PARG	PAR glycohydrolase
PARP	PAR polymerase
TRPM2	Melastatin-like transient receptor potential 2 channel

Introduction

Oxidative stress may induce DNA damage signaling in cells. Within seconds, poly(ADP-ribose)polymerase-1 (PARP-1) reacts to DNA nicks arising from oxidative damage, activating PARP-1. It signals downstream into DNA repair and cell death pathways [1–3]. PARP-1 produces large amounts of long and branched poly(ADP-ribose) molecules primarily on itself in an automodification reaction [1, 3]. The local polymer concentration increases several 100-fold, but decreases rapidly due to degradation by poly(ADP-ribose)glycohydrolase (PARG). PARG produces primarily ADP-ribose, albeit a few polymers may arise from endoglycosidic enzyme activity [4, 5].

The biological role of this dynamic poly(ADP-ribose) turnover is poorly understood. In several cell types, PARP-1 activation induces the release of apoptosis-inducing factor (AIF) from the inner mitochondrial membrane and its translocation to the nucleus, where it triggers chromatin condensation and large-scale DNA fragmentation [6–11]. AIF release involves proteolytic cleavage, either by calpain or by caspases pending on the type of cytotoxic stress and the cell type [8, 12–14]. By contrast, AIF translocation apparently may proceed also in the absence of proteolytic cleavage [15].

In vitro and in vivo evidence combined from different cell types indicates that poly(ADP-ribose) metabolism is involved in Ca^{2+} gating. Patch clamp experiments in lymphocytes showed that ADP-ribose addition to the inner chamber may activate a calcium channel at the outer cell membrane, termed melastatin-like transient receptor potential 2 channel (TRPM2) [16]. In microglia cells, ADP-ribose added to the intracellular pipette of a whole-cell-patch clamp assay causes TRPM2-mediated Ca^{2+} currents [17]. Oxidant-induced TRPM2 activation is inhibited by genetic or chemical disruption of PARP-1 activity in lymphocytes [16] and in a kidney cell line overexpressing TRPM2 [18].

In the present study, we used genetic knockout, RNAi, and chemical inhibitors to manipulate PARP-1, PARG, and TRPM2 to pinpoint the role of poly(ADP-ribose) metabolism in triggering calcium fluxes, caspase activation, AIF translocation, and cell death in a well-defined cell system after H_2O_2. We found that TRPM2 is the major channel for generating the Ca^{2+} influx after oxidative stress. Furthermore, abrogation of PARP-1 or PARG function affected the signal for TRPM2 activation, Ca^{2+} fluxes, caspase activation, AIF translocation, and cell death. The results suggest that PARG acts as the immediate upstream regulator of TRPM2 by generating ADP-ribose. Loading cells with ADP-ribose triggered a Ca^{2+} influx in the absence of oxidative damage. Thus, PARP-1 and PARG are an integral part of a cell death pathway that operates between five different cell compartments and communicates via three types of chemical messengers: a nucleotide, a cation, and proteins.

Materials and methods

Cell culture

Immortalized mouse embryonic fibroblasts (MEFs) of *wild-type* and *parp-1*$^{-/-}$ background were used. MEFs were cultured at 37°C in a water-saturated, 5% CO_2/95% air atmosphere, in complete Dulbecco's modified Eagle's medium (DMEM) containing 1 g/l glucose and supplemented with 10% (v/v) FBS and antibiotics (Invitrogen).

Calcium measurements and visualization

Twenty thousand cells per well in 96-well plates (Costar Corning Incorporated) were washed twice with 49 parts of calcium-free HBSS (0.49 mM $MgCl_2$, 0.41 mM $MgSO_4$, 5.33 mM KCl, 0.44 mM KH_2PO_4, 4.17 mM $NaHCO_3$, 137 mM NaCl, 0.34 mM Na_2HPO_4, 5.56 mM dextrose) supplemented with 1 part 1 M HEPES (pH 7.2) (assay buffer) containing $CaCl_2$ or not. Then, 100 µl Fluo-4-NW-dye-mix from Molecular Probes (Invitrogen) was added and incubated for 30 min at 37°C, followed by 30-min incubation in the dark at room temperature. Basic relative fluorescence units (RFU) before challenging the cells are shown in Supplementary Figures S4A, S4B. Changes in fluorescence from the Fluo-4-NW-dye quantify changes in intracellular calcium concentrations (excitation/emission 485/535 nm; slits 10/15 nm) in LS55 luminescence spectrometer (Perkin-Elmer) after H_2O_2. Calcium was monitored for 30 min with a measure frequency of 0.1 s. Each 50th time-point was taken for calculation. Every Fluo-4 analysis was monitored in parallel by at least one positive or negative control at each day of measurement. The statistical analysis is summarized in Supplementary Figure S4E.

For Ca^{2+} visualization, Fluo-4 loaded cells were analyzed 3 h after H_2O_2 treatment in a fluorescence microscope (Nikon). This time point was chosen according the offscale time in fluospectroscopic Fluo-4 analysis.

Loading of cells with ADP-ribose

For the Fluo-4 assays with pure ADP-ribose as a trigger for intracytosolic Ca^{2+} shifts, MEFs were loaded with monomeric ADP-ribose using the transfection reagent siPORT amine (Ambion). A total of 50 µl of 10 mM ADP-ribose in Fluo-4 assay buffer was incubated with 3 µl siPORT amine for 20 min at 37°C. Afterwards, this mixture was given on Fluo-4-loaded cells and preincubated together with cells for 25 min in a final volume of 200 µl (ADP-ribose at 2.5 mM) before intracytosolic Ca^{2+} shifts were monitored for 30 min as described above. Control experiments were performed with ADP-ribose solution without transfectant and Fluo-4 assay buffer with siPORTamine.

Chemicals

H_2O_2, *N*-(*N*-((Phenylmethoxy)carbonyl)-L-valyl)-phenylalaninal (MDL 28170) and ADP-ribose from SIGMA. 3-aminobenzamide (3-AB), 2-Methyl-3,5,7,8-tetrahydrothiopyranol-(4,3-d)-pyrimidine-4-one (DR2313), *N*-(6-Oxo-5,6-dihydro-phenanthridin-2-yl)-*N*,*N*-dimethylacetamide. HCl (PJ-34) from Alexis Biochemicals. 1,2-bis-(*o*-Aminophenoxy)-ethane-*N*,*N*,*N*′,*N*′-tetraaceticacid-tetraacetoxymethylester (BAPTA-AM) from Enzo Life Sciences. *N*-(*p*-Amylcinnamoyl)-anthranilicacid (ACA), *N*-(2-Quinolyl) valyl-aspartyl-(2,6-difluorophenoxy)methylketone (Q-VD-OPh) from Calbiochem. 2-(4-Morpholinyl)-8-phenyl-4H-1-benzopyran-4-one (LY294002) was obtained from Biaffin.

Inhibitors were dissolved in DMSO. All other chemicals were from Applichem, Fluka, Merck, or SIGMA.

Viability assay

Cells were seeded in 96-well plates (15,000 cells/well). H_2O_2 was diluted in OptiMEM and cells were treated with 50 µl/well for 1 h before 150 µl DMEM was added. After 20 h, medium was replaced with 200 µl DMEM 10% (v/v) Alamar blue (Serotec). After 4 h, fluorescence was monitored at 530-nm excitation and 590-nm emission wavelength (LS55 luminescence spectrometer, Perkin-Elmer).

Western-blot analyses and PAR immunofluorescence

The following primary antibodies were used: anti-PARP-1 (Alexis; C2-10, 1:5,000), anti-AIF (Serotec; 1:500), anti-GAPDH (Ambion; 1:1,00,000), anti-MnSOD (BD Biosciences; 1:1,000), anti-Topo-1 (BD Biosciences; 1:5,000), anti-α-tubulin (Sigma; 1:50,000), anti-PAR (Alexis; 1:1,000), anti-α-fodrin (ENZO Life Sciences; 1:8,000); anti-cleaved PARP (Asp214, 1:1,000), anti-caspase 12 (1:1,000), anti-cleaved caspase 9 (Asp353, 1:1,000), anti-cleaved caspase 6 (Asp162, 1:1,000), anti-cleaved caspase 3 (Asp175, 1:1,000), anti-caspase 9 (1:1,000), anti-caspase 6 (1:1,000), anti-caspase 3 (1:1,000), anti-phospho-PERK (Thr 980, 1:1,000, all from Cell Signaling). Anti-p-CaMKIIα (Thr 286-R, 1:1,000) and anti-CaMKII (M-176, 1:1,000) were obtained from Santa Cruz. Anti-calmodulin (1:1,000) was from Epitomics. All secondary antibodies were from Sigma. PAR detection after H_2O_2 exposure was performed by immunofluorescence microscopy [7].

Cellular subfractionation

This was performed as described before [7]. Briefly, MEFs were harvested and washed twice with Tris–HCl (pH 7.0), 0.13 M NaCl, 5 mM KCl, 7.5 mM $MgCl_2$. After incubation in 3.5 mM Tris–HCl (pH 7.8), 3 mM NaCl, 0.5 mM $MgCl_2$ for 5 min, cells were mechanically broken. The homogenate was mixed with one-ninth of the cell-volume of 0.35 M Tris–HCl (pH 7.8), 0.2 M NaCl, 50 mM $MgCl_2$, and spun for 3 min at 1,600 × *g*. The pellet (nuclei) was harvested directly in Laemmli buffer and the supernatant was recentrifuged under the same conditions. The final supernatant was spun at 13,000 × *g* for 1 min and the resulting mitochondrial pellet was washed once with 35 mM Tris–HCl (pH 7.8), 20 mM NaCl, 5 mM $MgCl_2$, then twice with 10 mM Tris–HCl (pH 7.4), 1 mM EDTA, 0.32 M sucrose and finally resuspended in Laemmli buffer. The procedure was performed at 4°C and a protease-inhibitor-cocktail (Complete™, EDTA-free, Roche) was added to all Tris-buffers.

PCR analysis

cDNA was produced from cells using the cells-to-cDNA II kit (Ambion) and used as templates for GAPDH and TRPM2 amplification in quantitative real-time PCR, with primers from Assays-on-demand Gene Expression products, in a reaction mixture including TaqMan Universal PCR Master Mix (Applied Biosystems). Real-time PCR experiments were carried out on an ABI PRISM 7700 cycler (95°C, 15 s; 60°C, 1 min; 40 cycles). For quantification, $\Delta\Delta C_t$ method was used. The TRPM2 primers were 5′-TACACTGACAGGCCACGGCT-3′ and 5′-CCAGCATGCACAGGATGATC-3′ (Microsynth). PCR analysis was performed in a reaction mixture including TaqMan Mix (Sigma) on Touchgene machine (TECHNE; 95°C, 5 min initial denaturation; 30 cycles of denaturation (95°C, 30 s), annealing (54°C, 30 s) and elongation (72°C, 1 min); 5 min of final extension at 70°C).

RNA interference

Poly(ADP-ribose)polymerase-1 targeting template sequences (siRNA-P1): 5′-AAACAGTAATAAGCGTCGCTCCCTTC-3′ (sense) and 5′-AAGAGCGACGCTTATTACTGTCCTGTCTC-3′ (antisense) [7]. The PARG targeting siRNA (siRNA-G) has been described earlier (Microsynth) [7, 19]. The siRNA against TRPM2 (siRNA-T2) was obtained from Applied Biosystems; 5′-GAGUCUACGUGGUCGAGUATT-3′ (sense) and 5′-UACUCGACCACGUAGACUCCA-3′ (antisense). All transfection experiments were performed with siPORT amine (Ambion) as transfection reagent under conditions described earlier [19].

NAD^+ determination

Measurement of NAD^+ was according to Jacobson and Jacobson [20]. Cells were in 96-well plates (25,000 cells/well). After treatment with 5 mM H_2O_2 in OptiMEM (50 µl/well), the cells were lysed with 50 µl ethanol supplemented with isonicotinic acid-hydrazide (20 mM, for 30 min at −80°C) at 10, 20, and 30 min. The assay volume of 300 µl/well contained 570 mM ethanol, 114 mM bicine pH 7.8, 4.8 mM EDTA and 1 mg/ml BSA. The color change of thiazolyl-blue-tetrazolium-bromide (MTT, 0.48 mM, SIGMA) was measured 15 min after ADH was added (6 µg/ml, Roche) in a UV spectrometer (Bio-Rad) at 570 nm. A calibration curve was performed in parallel.

Statistical analysis

Results are shown as mean ± SD of at least three independent experiments. The significance of differences was estimated by ANOVA followed by the method of Kolmogorov and Smirnov. $p < 0.05$ was considered significant. All statistical analyses were performed with InStat3 software (GraphPad Software).

Results

Oxidative stress induces PAR formation, Ca^{2+} fluxes, and cell death

Cell death induced by H_2O_2 is preceded by PAR formation and Ca^{2+} fluxes in mouse embryonic fibroblasts (MEFs) (Fig. 1). Cell death was dose-dependent (Fig. 1a), reducing viable cells by 29.8 ± 7.4% at 0.5 mM and 68.5 ± 4.1% at 5 mM H_2O_2 within 20 h. PAR induction (Fig. 1b, c) and Ca^{2+} gating into the cytosol (Fig. 1d–f) were observed within min of oxidative insults. All cytosolic Ca^{2+} could be completely quenched by a pretreatment with the Ca^{2+} chelator BAPTA (Suppl. Fig. S1A) as tested with the Fluo-4 assay. Figure 1d shows the effects of 0.5 and 5 mM H_2O_2 on intracellular Ca^{2+} levels over 30 min. Figure 1e shows the impact of 5 mM H_2O_2, performed in presence or absence of 1 mM exogenous Ca^{2+}. Moreover, 5 mM exogenous Ca^{2+} could not further promote the level of Ca^{2+} signals obtained with 1 mM Ca^{2+} (Suppl. Fig. S1D).

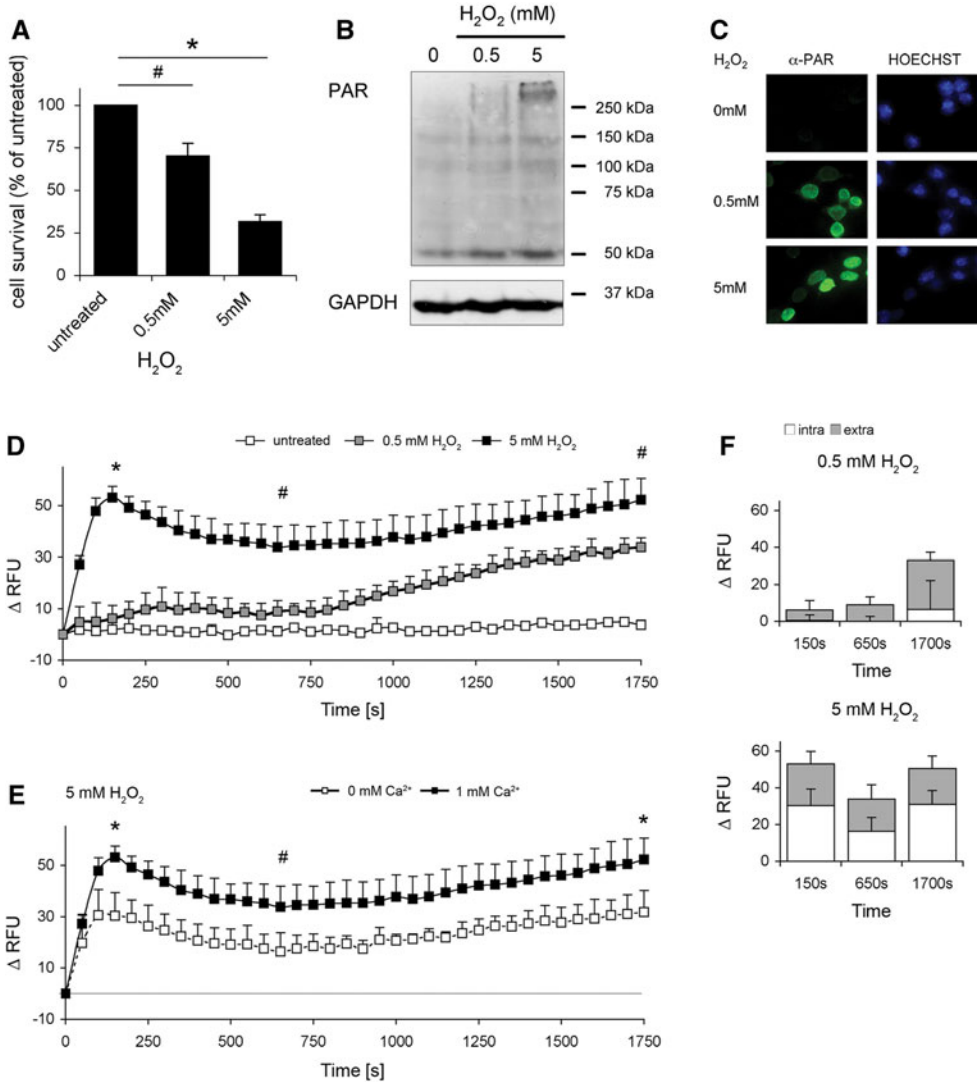

Fig. 1 Effects of H_2O_2 on poly(ADP-ribose), Ca^{2+} levels, and cell survival. **a** *Wild-type* MEFs were treated with 0.5 or 5 mM of H_2O_2 for 20 h. Cell survival was monitored by Alamar blue assay. Results represent the mean ± SD for at least three independent experiments ($^{\#}p < 0.0025$; $^{*}p < 0.0001$; *t* test). **b** Western-blot analysis of PAR after 15 min of H_2O_2 treatment. GAPDH is loading control. **c** PAR detection by immunofluorescence after 30 min of H_2O_2 treatment. HOECHST staining is also shown. **d** Fluo-4 assay of H_2O_2-challenged cells. Changes of cytosolic Ca^{2+} were monitored directly after treatment for 30 min by fluorescence spectrometry and are expressed as ΔRFU compared to basic levels. Results represent mean ± SD ($^{\#}p < 0.005$; $^{*}p < 0.0001$; $n = 4$; *t* test). **e** Ca^{2+} determination after 5 mM H_2O_2 with and without extracellular Ca^{2+} ions. Shown are ΔRFUs and *error bars* ($^{\#}p < 0.025$; $^{*}p < 0.001$; $n = 4$; *t* test). **f** Comparison of Ca^{2+} from intra- and extracellular sources after 0.5 or 5 mM of H_2O_2. Shown are ΔRFUs with or without Ca^{2+} in the buffer at characteristic time points (150, 650, and 1,700 s; $n = 4$)

Cytosolic Ca^{2+} also increased in the absence of exogenous Ca^{2+}, suggesting that Ca^{2+} was released from endogenous Ca^{2+} stores. Ca^{2+}-free conditions did not affect cell viability or baseline Ca^{2+} levels (Suppl. Fig. S1B, S1C). Figure 1f shows a comparison of Ca^{2+} from internal and external sources. Low levels of H_2O_2 (0.5 mM) cause exclusively Ca^{2+} influxes from the extracellular milieu, rising continuously up to 30 min. High levels of H_2O_2 (5 mM) lead to Ca^{2+} shifts from extra- and intracellular sources, producing a peak at 150 s, a trough at 650 s, followed by a continuous rise of Ca^{2+} (Fig. 1d–f). Compared to other cell organelles, the basal Ca^{2+} concentration of endoplasmic reticulum is 5,000-fold higher than cytosolic Ca^{2+}, and hence is the most likely source of intracellular Ca^{2+} releases [21]. However, the Ca^{2+} peak at 150 s could be addressed to PI3K (phosphoinositide 3-kinase) activity as it could be reduced by the parallel incubation with its inhibitor LY294002 (50 μM, data not shown).

PARP-1 inhibition by chemicals, RNAi and knockout reduce H_2O_2 cytotoxicity and cytosolic Ca^{2+} shifts

Using chemical inhibition, RNAi silencing or genetic knockout of *parp-1*, we determined the consequences on cytosolic Ca^{2+} shifts and cell survival (Fig. 2). Regardless of the type of PARP-1 abrogation, H_2O_2-induced cytotoxicity (Fig. 2a) and cytosolic Ca^{2+} increases (Fig. 2b–g) were reduced. In particular, PARP inhibitor 3-aminobenzamide (3-AB) decreased cytosolic Ca^{2+} shifts up to 30 min (Fig. 2b), and this was observed over a dose range of 1–10 mM (Suppl. Fig. S2C). Inhibition of PARP reduced Ca^{2+} levels after H_2O_2 (Fig. 2c). 3-AB was not toxic per se nor did it affect the expression of PARP-1 (Suppl. Fig. S2A, S2B). Moreover, the presence or absence of Ca^{2+} did not alter the baseline levels (Suppl. Figs. S2D, S2E, S4A). These results were confirmed with other PARP inhibitors: cells grown in the presence of 5 μM PJ-34 (Fig. 2d; Suppl. Fig. S4A) or 100 μM DR2313 (Fig. 2e; Suppl. Fig. S4A) showed similar Ca^{2+} shifts after H_2O_2 as those grown in 3 mM 3-AB (Fig. 2b).

As expected, RNAi silencing of *parp-1* reduced PARP-1 protein to very low levels (Fig. 2f, Western blot) and caused a further reduction of Ca^{2+} signals from extracellular space after an oxidative insult (Fig. 2c, f). Using a third approach, we determined Ca^{2+} shifts in *parp-1*$^{-/-}$ cells (Fig. 2g, 3a). The *parp-1* gene knockout was verified by Western blot (Fig. 2g) and the inability to convert NAD^+ into PAR after H_2O_2 (Suppl. Fig. S2G). The reduction of the basal NAD^+ content in *parp-1*$^{-/-}$ cells challenged with 5 mM H_2O_2 is likely due to PARP-2 activity [33–35]. Evidently, MEFs lacking PARP-1 are resistant to H_2O_2-induced cytotoxicity (Fig. 2a) and did not show any Ca^{2+} influx from the extracellular space (Fig. 2g; Suppl. Figs. S2F, S2H, S2I, S4A).

To further address the role of PARP-1 in Ca^{2+} signaling, Ca^{2+} levels were visualized in *parp-1*$^{-/-}$ versus *wild-type* cells by fluorescence microscopy after 5 mM H_2O_2 (Fig. 3a). While detectable Ca^{2+} levels were seen in *wild-type* cells, *parp-1*$^{-/-}$ failed to show a signal. The amount of cytosolic Ca^{2+} after H_2O_2 is of biological relevance because the Ca^{2+}/calmodulin dependent protein kinase II (CaMKII) becomes phosphorylated only in *wild-type* cells (Fig. 3c). The expression level of calmodulin is similar in *wild-type* and *parp-1*$^{-/-}$ cells (Suppl. Fig. S3A). Interestingly, the marginal PARP-1-independent Ca^{2+} released from intracellular sources displays endoplasmic reticulum stress as assayed by the phosphorylation of protein kinase-like endoplasmic reticulum kinase [22] (PERK, Fig. 3b). Our findings suggest that PARP-1 activity is required for the influx of Ca^{2+} from the extracellular space leading to Ca^{2+} signaling after an oxidative insult.

PARP-1-dependent Ca^{2+} gating initiates downstream factors in cell death

We next determined the PARP-1 dependency of extracellular Ca^{2+} influxes on the activation of calpain and caspases, which is a controversial issue in AIF release [8, 12–15, 23–25]. A total of 5 mM H_2O_2 induced activation of calpain as determined by α-fodrin cleavage [14]. However, this activation was independent of PARP-1 (Fig. 3d). By contrast, the activation of caspases 3, 6, and 9 was clearly reduced in *parp-1*$^{-/-}$ cells (Fig. 3e), some of them being implicated in AIF release from the inner mitochondrial membrane [7, 12, 14]. Caspase 12 activation was identical in PARP-1-proficient and -deficient cells (Fig. 3e), which is in line with results of Fig. 3d and the literature demonstrating intracellular Ca^{2+} currents and calpain induction in various cell-death models connected with stress to endoplasmic reticulum [26–28]. The expression levels of caspases were identical in *wild-type* and *parp-1*$^{-/-}$ cells (Suppl. Fig. S3C). A parallel inhibition of calpains (MDL 28170) or caspases (Q-VD-OPh) could reduce the specific proteolytic truncates (Suppl. Fig. S3B, S3D). Hence we conclude that the PARP-1 independent intracellular Ca^{2+} shifts are sufficient for calpain activation and that the activation of caspases requires PARP-1.

The next series of experiments examined AIF translocation in cells silenced for *parp-1*. While AIF migrates from mitochondria to the nucleus in H_2O_2-challenged control cells (siRNA C), the translocation was inhibited in cells silenced for PARP-1 (siRNA 1, Fig. 3f). As a final consequence, cells with an impaired PARP-1 system showed an increased survival rate after an oxidative challenge (Fig. 2a).

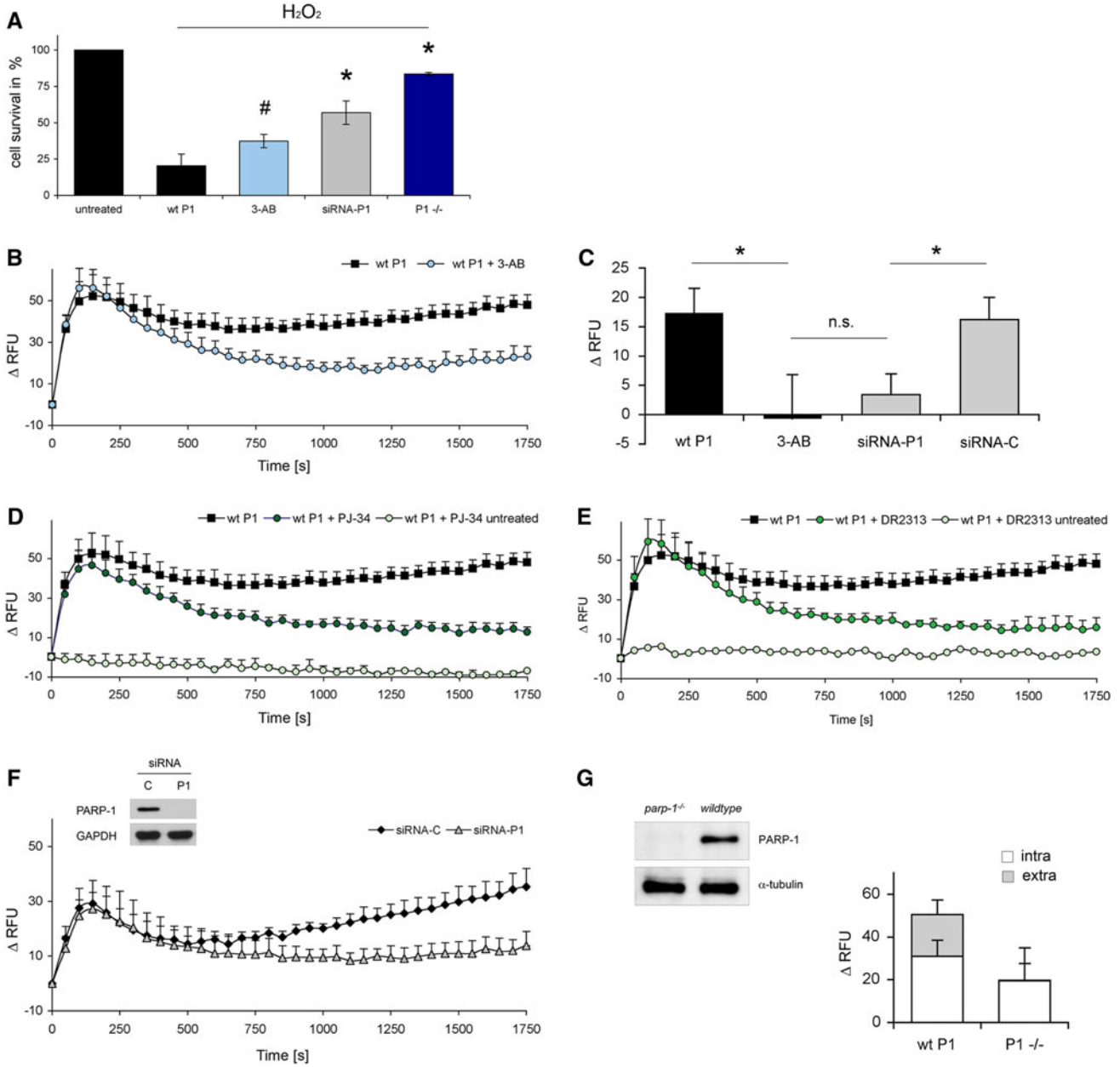

Fig. 2 Inhibition of PARP-1 protects cells against cytotoxicity and reduces Ca^{2+} levels after H_2O_2. **a** *Wild-type* (wt P1), *parp-1*$^{-/-}$ MEFs (P1$^{-/-}$) and cells incubated with 3 mM 3-AB overnight (3-AB) or silenced for the *parp-1* gene (siRNA-P1) were challenged with 5 mM H_2O_2. After 20 h, cytotoxicity was determined by Alamar blue assay (mean ± SD; $^{\#}p < 0.025$; $^{*}p < 0.0025$; $n \geq 3$; *t* test). **b** Ca^{2+} assays of *wild-type* (wt P1) and 3-AB (3 mM) treated cells. MEFs were monitored for Ca^{2+} alterations after 5 mM H_2O_2 (mean ± SD; $n \geq 4$). **c** Differences in cytosolic Ca^{2+} levels after 5 mM H_2O_2 in *wild-type* (wt P1), 3-AB (3 mM) treated cells and MEFs silenced with siRNA against *parp-1* (siRNA-P1) as well as cells transfected with a control siRNA (siRNA-C) after 1,700 s (mean ± SD; $^{*}p < 0.025$; $n \geq 3$; *t* test). **d** Ca^{2+} assays of *wild-type* cells (wt P1) and cells with 5 μM of PARP-inhibitor PJ-34 (wt P1 + PJ-34) after 5 mM H_2O_2 (mean ± SD; $n \geq 4$). Values of controls (wt P1 + PJ-34 untreated) are shown too (mean ± SD; $n = 2$). **e** Effect of PARP-inhibitor DR2313 (100 μM) on Ca^{2+} shifts after 5 mM H_2O_2 (mean ± SD; $n \geq 3$). Ca^{2+} values of controls (wt P1 + DR2313 untreated) are presented ($n = 1$). **f** MEFs were silenced for the *parp-1* gene (siRNA-P1) and subjected to Fluo-4 assay. Cells treated with a control RNA sequence (siRNA-C) were analyzed in parallel. Shown are the mean ± SD ($n = 4$). Silencing efficacy was determined by Western blot with GAPDH as loading control. **g** Comparison of Ca^{2+} levels from intra- and extracellular sources after 5 mM H_2O_2 in *wild-type* (wt P1) and *parp-1*$^{-/-}$ (P1$^{-/-}$). Shown are ΔRFUs (mean ± SD; $n \geq 4$) of Ca^{2+} assays with or without Ca^{2+} in the buffer as indicated at 1,700 s after treatment. Western-blot analysis for PARP-1 protein is shown too with α-tubulin as loading control

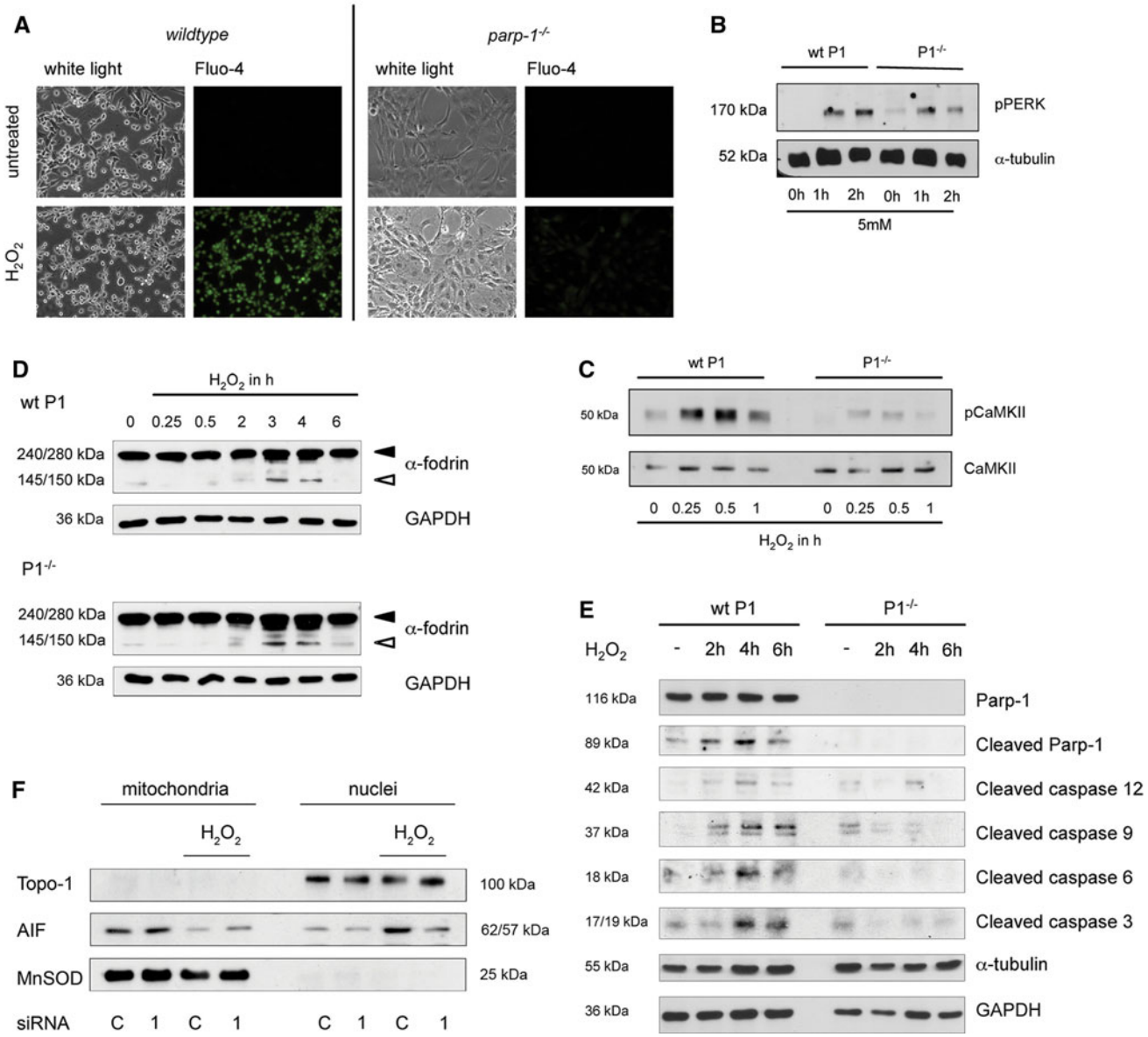

Fig. 3 Effects of H_2O_2 on cytosolic Ca^{2+} and Ca^{2+} signaling. **a** Microscopic visualization of intracellular Ca^{2+} shifts after 5 mM H_2O_2 (3 h) using the Ca^{2+} indicator Fluo-4 in *wild-type* and *parp-1*$^{-/-}$ cells. **b** Western-blot analysis of phosphorylated PERK protein with α-tubulin as loading control. *Wild-type* (wt P1) and *parp-1* knockout MEFs (P1$^{-/-}$) were treated for the indicated timepoints with 5 mM H_2O_2. **c** Western-blot analysis of phosphorylated CaMKII in H_2O_2 (5 mM) treated *wild-type* (wt P1) and *parp-1*$^{-/-}$ MEFs (P1$^{-/-}$) at the indicated timepoints. CaMKII is shown as a loading control. **d** Western-blot analysis of α-fodrin in *wild-type* (wt P1) and *parp-1* knockout (P1$^{-/-}$) cells. Cells were treated with 5 mM H_2O_2 for the indicated time points, harvested and subjected to Western-blot analysis. GAPDH is loading control. **e** Activation of caspases and appearance of cleaved PARP-1 after 5 mM H_2O_2 is shown in Western-blot analysis of whole cell lysates prepared from *wild-type* (wt P1) and *parp-1* knockout (P1$^{-/-}$) cells at the indicated timepoints. GAPDH and α-tubulin are shown as loading controls. **f** Translocation of AIF after H_2O_2 insult was determined in *wild-type* cells silenced for the *parp-1* gene by RNAi (siRNA 1) and cells silenced with a scrambled control siRNA (siRNA C). After 6 h treatment with 5 mM H_2O_2, cells were subjected to subcellular fractionation and immunoblotting. Topo-1 and MnSOD protein are also shown

TRPM2 is the primary channel for PARP-1-dependent extracellular Ca^{2+} gating

In order to determine the type of channel involved in Ca^{2+} gating, RNAi experiments were performed. RNAi silencing of TRPM2 channel reduced Ca^{2+} to the levels resistant to PARP-1/PARG regulation (Fig. 4a; Suppl. Figs. S2N, S4B), suggesting a primary role of this channel in death signaling. Likewise, *N*-(*p*-Amylcinnamoyl)anthranilic acid (ACA), a broad spectrum TRP channel blocker with an IC_{50} of 1.7 μM for TRPM2 [29–31], confirmed this finding (Fig. 4b; Suppl. Fig. S4A). Thus, TRPM2 seems to account

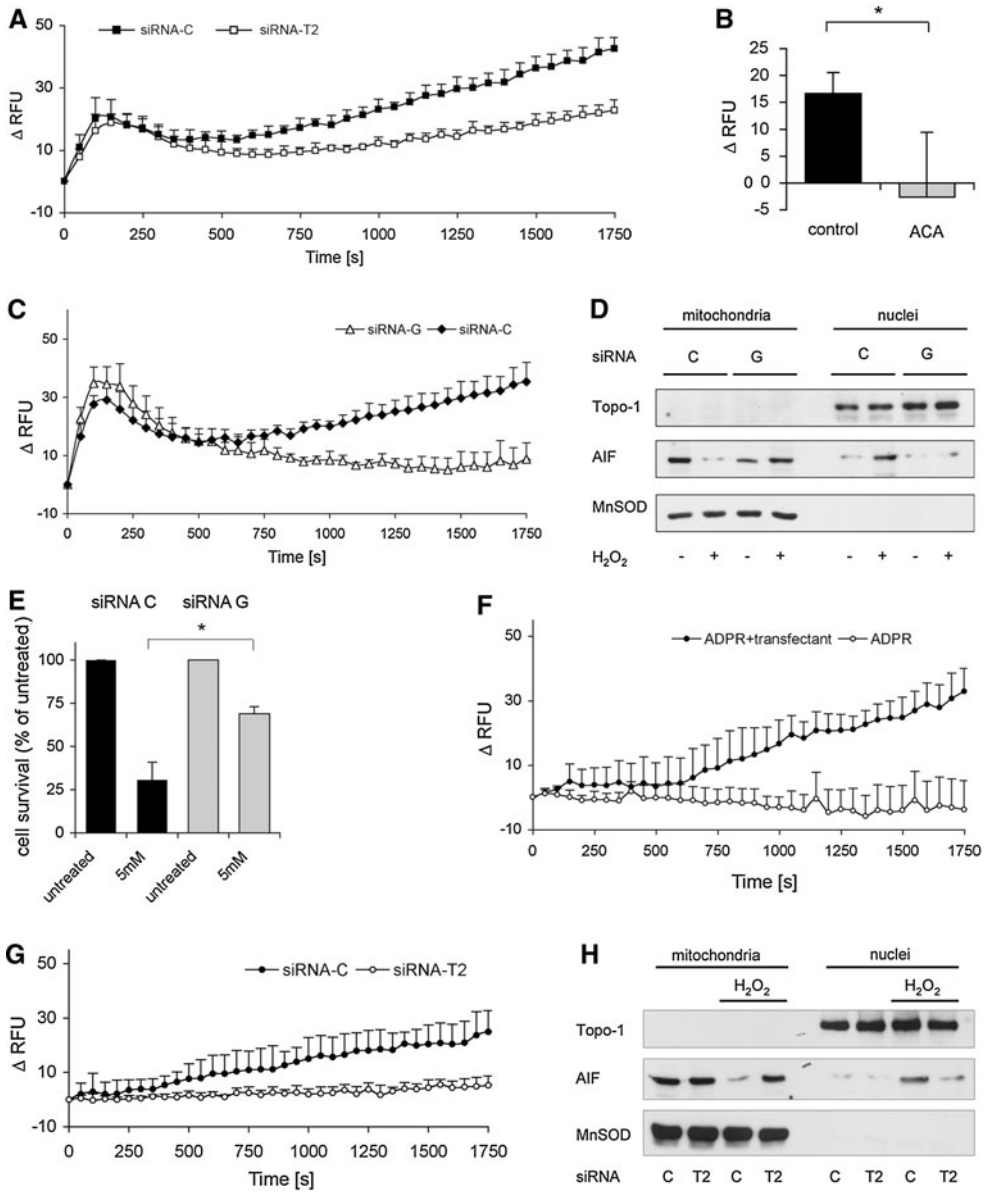

Fig. 4 PARG and TRPM2 are required for Ca^{2+} gating. **a** Fluo-4 assay in cells silenced (siRNA-T2) or unsilenced (siRNA-C) for the *trpm2* gene after 5 mM H_2O_2 (mean ± SD; $n = 3$). **b** Differences in extracellular Ca^{2+} entry after 5 mM H_2O_2 in control and ACA-treated cells (5 μM ACA with additional pretreatment of ACA for 5 min) after 1,700 s (mean ± SD; $n \geq 4$; $^*p < 0.001$; *t* test). **c** MEFs were silenced for the *parg* gene (siRNA-G) and subjected to Fluo-4 assay. Cells treated with a control RNA sequence (siRNA-C) were analyzed in parallel. Shown are the mean ± SD ($n \geq 3$). **d** Western-blot analysis of AIF translocation from mitochondrial to the nuclear fraction. Control (siRNA-C) and *parg* silenced cells (siRNA-G) treated with 5 mM H_2O_2 or solvent controls were subjected to subcellular fractionation at 6 h. Topo-1 and MnSOD served as loading and fraction purity controls. **e** Control MEFs (siRNA-C) and *parg*-silenced cells (siRNA-G) were challenged with 5 mM H_2O_2. After 20 h, survival rates were determined by Alamar blue dye. Shown are the results as percent of the untreated control cells (mean ± SD; $^*p < 0.005$; $n = 3$; *t* test). **f** MEFs were loaded with ADP-ribose (2.5 mM ADP-ribose in assay buffer + transfectant) before subjected to the Fluo-4 assay (mean ± SD; $n = 3$). ADP-ribose (2.5 mM) without transfectant was used as a control (mean ± SD; $n = 3$). **g** Control (siRNA-C) and *trpm2*-silenced cells (siRNA-T2) were loaded with ADP-ribose (2.5 mM ADP-ribose in assay buffer + transfectant) before subjected to the Fluo-4 assay (mean ± SD; $n = 2$). **h** Western-blot analysis of AIF translocation from mitochondrial to the nuclear fraction. Control (siRNA-C) and *trpm2*-silenced cells (siRNA-T2) treated with 5 mM H_2O_2 or solvent controls were subjected to subcellular fractionation at 6 h. Topo-1 and MnSOD served as loading controls

for the extracellular Ca^{2+} transients in cells exposed to 5 mM H_2O_2. We then examined the possibility that PARP-1 could affect the expression levels of TRPM2 in MEFs. Supplementary Figure S2L and S2M show that TRPM2 expression was identical in *wild-type* and *parp-1*$^{-/-}$ MEFs as determined by RT-PCR and endpoint PCR analysis.

PARG generates ADP-ribose, the signal for TRPM2 activation and downstream events in oxidant-induced cell death

We next hypothesized that PARG could control Ca^{2+} shifts by converting poly(ADP-ribose) into ADP-ribose, a possible activator of TRPM2 channels in vitro. First, we analyzed Ca^{2+} in MEFs with a silenced *parg* gene (siRNA-G) after 5 mM H_2O_2 and compared them with cells transfected with control siRNA (siRNA-C, Fig. 4c; Suppl. Figs. S2J, S2K, S4B). We published earlier that *parg* silencing is characterized by a reduced level of *parg* mRNA, PARG protein as well as enzymatic activity and results in a transient accumulation of long PAR molecules after oxidative stress [19]. Ca^{2+} shifts obtained in *parg* silenced cells were similar to those previously described in cells with abrogated TRPM2 (Fig. 4a) or PARP-1 function (Fig. 2b–g). Thus, PARG is the major regulator of TRPM2-mediated Ca^{2+} fluxes in cells subjected to oxidative stress. As expected, the reduced Ca^{2+} shifts resulted in an impaired AIF translocation from mitochondria to nucleus (Fig. 4d) and in a reduced cytotoxicity after 5 mM (Fig. 4e). To directly demonstrate the role of ADP-ribose as TRPM2 activator, cells were loaded with the nucleoside and intracellular Ca^{2+} levels monitored (Fig. 4f). The results show that ADP-ribose per se can cause a rise in cytosolic Ca^{2+} in the complete absence of oxidative stress. This effect is not seen when ADP-ribose was added in the absence of transfection agent or with transfection agent and assay buffer (Suppl. Fig. S4D). In fact, when MEFs were silenced for the *trpm2* gene, transfected ADP-ribose could not generate a cytosolic Ca^{2+} shift (Fig. 4g), indicating an important role of TRPM2 in Ca^{2+} gating through intracellular ADP-ribose as second messenger. Moreover, the translocation of AIF after oxidative stress was impaired after silencing of *trpm2* (Fig. 4h). Interestingly, RNAi against *trpm2* could not rescue the cells from cell death (data not shown), suggesting the involvement of an AIF-independent branch of the cell death pathway, as has been reported [57].

Discussion

Cell death following oxidative stress involves diverse 'death signals'. It is not clear how these signals cooperate between several cell compartments to trigger cell death in a specific cell type [2, 28, 32]. Our results link PARP-1 and PARG activity, TRPM2-gated Ca^{2+}, and caspase activation with AIF translocation and cell death. Figure 5 assembles the signaling elements into a schematic pathway. The first step is the generation of DNA damage by oxidative stress (H_2O_2). This activates PARP-1 generating a burst of PAR synthesis, a Ca^{2+} influx and cell death (Fig. 1). Besides PARP-1, PARP-2 has been shown to be stimulated by genotoxins in vitro and in vivo [33–35]. However, PARP-1 is the main enzyme producing PAR, accounting for >99% of PAR in cells after genotoxic insults [36–38]. Our results demonstrate that regardless of the method of PARP-1 abrogation, the Ca^{2+} influx and cell death was reduced (Fig. 2). Likewise, caspase activation and AIF translocation from mitochondria to the nucleus was suppressed (Fig. 3). Importantly, RNAi against TRPM2 or PARG blocked the Ca^{2+} influx suggesting that TRPM2 was the primary Ca^{2+} channel for cell death signaling under PARG control. PARG-silencing also prevented AIF translocation and cell death (Fig. 4). Finally, cells loaded with ADP-ribose, the enzymatic product of PARG activity, showed a distinct Ca^{2+} influx even in the absence of oxidative damage (Fig. 4f). We conclude that PARG acts as the immediate upstream regulator of TRPM2 by generating ADP-ribose. This is compatible with patch-clamp experiments showing activation of TRPM2 when ADP-ribose was included in the intracellular pipette [16, 39].

TRPM2 contains a NUDIX box sequence motif in the C-terminal domain with a binding site for ADP-ribose. The EC_{50} for ADP-ribose is 90 μM [40, 41], which is slightly above the intracellular ADP-ribose concentration (in the range of 5 and 90 μM) [42, 43]. Thus, TRPM2 gating is very sensitive to changes in intracellular ADP-ribose concentrations due to oxidant-induced stimulation of PARP-1 and PARG activity. In fact, when TRPM2 is silenced or inhibited, the gating activity for extracellular Ca^{2+} is abolished (Fig. 4a, b). Accordingly, both the level and the rate of Ca^{2+} increase depended on the dose of H_2O_2 (Fig. 1d). The resulting Ca^{2+} influx from the extracellular milieu (~1 mM Ca^{2+}) merges with the low concentration of the cytosolic pool (~100 nM Ca^{2+}) [21], which is in the detection range of the Ca^{2+} probe Fluo-4 (K_D for Ca^{2+} 345 nM) [44] used in this study. A low dose of H_2O_2 is sufficient to induce extracellular Ca^{2+} shifts (Fig. 1f). Nevertheless, we detected an additional Ca^{2+} shift from intracellular stores in cells treated with high doses of H_2O_2 (Fig. 1e, f; Suppl. Fig. S4C). The trough after the initial rise (Figs. 1, 2, 4) could reflect the Ca^{2+} reuptake into intracellular Ca^{2+} stores [21]. Release of Ca^{2+} from intracellular Ca^{2+} depots has been reported in pancreatic acinar cells [45], neutrophils [46], hepatocytes [47], and in LPS-challenged microglia [17] cells after H_2O_2.

An elevated intracellular Ca^{2+} level was shown in relationship with two types of cell death proteases involved in AIF processing and translocation from the mitochondria to the nucleus: calpain [8, 13, 23, 24] and caspases [12, 14, 25]. Both types were activated (Fig. 3) but only the activation of caspases 3, 6, and 9—not 12—was PARP-1-

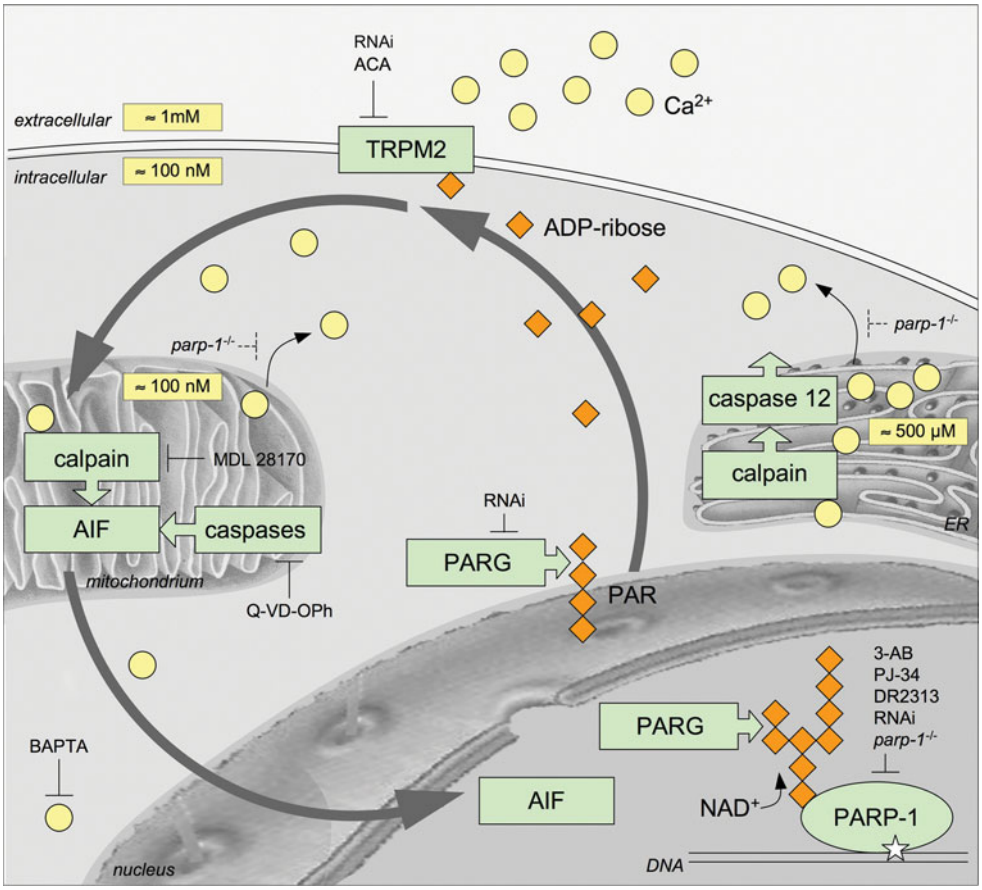

Fig. 5 PARP-1 and PARG control TRPM2 in a multicompartment pathway to cell death. Oxidative DNA damage activates PARP-1, which converts NAD^+ into PAR. PARG degrades PAR and produces free ADP-ribose monomers, which are released into the cytosol. There they activate intermembrane TRPM2 channels and induce a Ca^{2+} influx. Ca^{2+} activates calpains and subsequently caspases, but only the latter depends on PARP-1. Caspases become activated as a cascade (9 → 6 → 3) cleaving mitochondrial AIF, which then translocates to the nucleus to cause DNA fragmentation, chromatin condensation, and cell death

dependent (Fig. 3e). Since AIF translocation from mitochondria to the nucleus was strictly PARP-1-dependent (Fig. 3f), we conclude that Ca^{2+} induces a signaling pathway leading to the consecutive activation of caspases 9, 6, and 3 (Fig. 3e) and this in turn releases AIF from the inner mitochondrial membrane to translocate to the nucleus (Fig. 3f) and to induce cell death. By contrast, calpain activation by H_2O_2-induced Ca^{2+} fluxes is not dependent on PARP-1 (Fig. 3d). Consistent with our observations, the PARP-1 dependency of AIF translocation has been demonstrated in other cells, but attributed to the action of polymeric and not monomeric ADP-ribose [6, 7, 10]. Accordingly, *parg* silencing prevented AIF translocation and cell death as well (Fig. 4d, e). This may explain why PARG inhibition or genetic disruption has a cytoprotective effect in various cell types [19, 48–50].

The H_2O_2-induced Ca^{2+} influx has been described before in cells overexpressing the TRPM2 channel [16, 41, 51] as well as in *trpm2*$^{-/-}$ cells restored with TRPM2 [52]. Beside H_2O_2, cytoplasmic Ca^{2+} and ADP-ribose act as coactivators of TRPM2 gating [17, 40, 41, 53]. ADP-ribose may be converted into AMP by pyrophosphatase activity of the NUDT9 domain and thereby initiate Ca^{2+} gating via TRPM2 [40, 54]. Formentini et al. [55] recently described a functional role for NUDIX hydrolases after PARP-1 hyperactivation, resulting in accumulation of AMP. However, enhancing the enzymatic activity of the NUDIX box abolishes ADP-ribose gating of TRPM2, confirming that ADP-ribose itself, and not its degradation product, is involved in TRPM2 gating (reviewed by Hecquet et al. [56]).

Some of our observations seem to be in contrast to published results. Calpain has been implicated in AIF cleavage prior to its release from the inner mitochondrial membrane. While we could confirm calpain activation in H_2O_2-treated MEFs, which was inhibited by calpain inhibitor MDL 28170, it was unaffected by deletion of the *parp-1*$^{-/-}$ gene (Fig. 3d; Suppl. Fig. S3B). The discrepancy could be explained by differences in cell death inducers, i.e., an alkylating agent [8] versus H_2O_2 (this study), and hence differences in cell death signaling. Moreover, a recent report confirms that calpain is not required for PARP-1- and AIF-dependent cell death [25]. Likewise, PARP-1-dependent cell death may also progress in an AIF-independent manner as shown by Tang et al. [57] in cells deficient in base excision repair. More studies are needed to understand the complexity of molecular interactions of PAR in cell death.

We conclude that the two major PAR metabolizing enzymes PARP-1 and PARG control a cell death pathway

that operates between five different cell compartments and communicates via three types of chemical messengers: a nucleotide, a cation, and proteins. PARP-1 is producing the upstream death signal poly(ADP-ribose), which is converted by PARG into ADP-ribose, to specifically activate TRPM2 with concomitant cytosolic Ca^{2+} shifts that trigger caspases, AIF translocation, and cell death.

Acknowledgements This work was supported by the Vetsuisse Faculty, the Swiss National Science Foundation, and a grant from the Lotte and Adolf Hotz-Sprenger Foundation, Zurich, awarded to F.R.A.

References

1. Ame JC, Spenlehauer C, de Murcia G (2004) The PARP superfamily. Bioessays 26:882–893
2. Hassa PO, Haenni SS, Elser M, Hottiger MO (2006) Nuclear ADP-ribosylation reactions in mammalian cells: where are we today and where are we going? Microbiol Mol Biol Rev 70:789–829
3. Schreiber V, Dantzer F, Ame JC, de Murcia G (2006) Poly(ADP-ribose): novel functions for an old molecule. Nat Rev Mol Cell Biol 7:517–528
4. Brochu G, Duchaine C, Thibeault L, Lagueux J, Shah GM, Poirier GG (1994) Mode of action of poly(ADP-ribose) glycohydrolase. Biochim Biophys Acta 1219:342–350
5. Davidovic L, Vodenicharov M, Affar EB, Poirier GG (2001) Importance of poly(ADP-ribose) glycohydrolase in the control of poly(ADP-ribose) metabolism. Exp Cell Res 268:7–13
6. Andrabi SA, Kim NS, Yu SW, Wang H, Koh DW, Sasaki M, Klaus JA, Otsuka T, Zhang Z, Koehler RC, Hurn PD, Poirier GG, Dawson VL, Dawson TM (2006) Poly(ADP-ribose) (PAR) polymer is a death signal. Proc Natl Acad Sci USA 103:18308–18313
7. Cohausz O, Blenn C, Malanga M, Althaus FR (2008) The roles of poly(ADP-ribose)-metabolizing enzymes in alkylation-induced cell death. Cell Mol Life Sci 65:644–655
8. Moubarak RS, Yuste VJ, Artus C, Bouharrour A, Greer PA, Menissier-de Murcia J, Susin SA (2007) Sequential activation of poly(ADP-ribose) polymerase 1, calpains, and Bax is essential in apoptosis-inducing factor-mediated programmed necrosis. Mol Cell Biol 27:4844–4862
9. Susin SA, Lorenzo HK, Zamzami N, Marzo I, Snow BE, Brothers GM, Mangion J, Jacotot E, Costantini P, Loeffler M, Larochette N, Goodlett DR, Aebersold R, Siderovski DP, Penninger JM, Kroemer G (1999) Molecular characterization of mitochondrial apoptosis-inducing factor. Nature 397:441–446
10. Yu SW, Andrabi SA, Wang H, Kim NS, Poirier GG, Dawson TM, Dawson VL (2006) Apoptosis-inducing factor mediates poly(ADP-ribose) (PAR) polymer-induced cell death. Proc Natl Acad Sci USA 103:18314–18319
11. Yu SW, Wang H, Poitras MF, Coombs C, Bowers WJ, Federoff HJ, Poirier GG, Dawson TM, Dawson VL (2002) Mediation of poly(ADP-ribose) polymerase-1-dependent cell death by apoptosis-inducing factor. Science 297:259–263
12. Arnoult D, Parone P, Martinou JC, Antonsson B, Estaquier J, Ameisen JC (2002) Mitochondrial release of apoptosis-inducing factor occurs downstream of cytochrome c release in response to several proapoptotic stimuli. J Cell Biol 159:923–929
13. Cao G, Xing J, Xiao X, Liou AK, Gao Y, Yin XM, Clark RS, Graham SH, Chen J (2007) Critical role of calpain I in mitochondrial release of apoptosis-inducing factor in ischemic neuronal injury. J Neurosci 27:9278–9293
14. Diwakarla S, Nagley P, Hughes ML, Chen B, Beart PM (2009) Differential insult-dependent recruitment of the intrinsic mitochondrial pathway during neuronal programmed cell death. Cell Mol Life Sci 66:156–172
15. Yu SW, Wang Y, Frydenlund DS, Ottersen OP, Dawson VL, Dawson TM (2009) Outer mitochondrial membrane localization of apoptosis-inducing factor: mechanistic implications for release. ASN Neuro. doi: 10.1042/AN20090046
16. Buelow B, Song Y, Scharenberg AM (2008) The Poly(ADP-ribose) polymerase PARP-1 is required for oxidative stress-induced TRPM2 activation in lymphocytes. J Biol Chem 283:24571–24583
17. Kraft R, Grimm C, Grosse K, Hoffmann A, Sauerbruch S, Kettenmann H, Schultz G, Harteneck C (2004) Hydrogen peroxide and ADP-ribose induce TRPM2-mediated calcium influx and cation currents in microglia. Am J Physiol Cell Physiol 286:C129–C137
18. Fonfria E, Marshall IC, Benham CD, Boyfield I, Brown JD, Hill K, Hughes JP, Skaper SD, McNulty S (2004) TRPM2 channel opening in response to oxidative stress is dependent on activation of poly(ADP-ribose) polymerase. Br J Pharmacol 143:186–192
19. Blenn C, Althaus FR, Malanga M (2006) Poly(ADP-ribose) glycohydrolase silencing protects against H_2O_2-induced cell death. Biochem J 396:419–429
20. Jacobson EL, Jacobson MK (1997) Tissue NAD as a biochemical measure of niacin status in humans. Methods Enzymol 280:221–230
21. Szabadkai G, Duchen MR (2008) Mitochondria: the hub of cellular Ca^{2+} signaling. Physiology (Bethesda) 23:84–94
22. Harding HP, Zhang Y, Ron D (1999) Protein translation and folding are coupled by an endoplasmic-reticulum-resident kinase. Nature 397:271–274
23. Churbanova IY, Sevrioukova IF (2008) Redox-dependent changes in molecular properties of mitochondrial apoptosis-inducing factor. J Biol Chem 283:5622–5631
24. Norberg E, Gogvadze V, Ott M, Horn M, Uhlen P, Orrenius S, Zhivotovsky B (2008) An increase in intracellular Ca^{2+} is required for the activation of mitochondrial calpain to release AIF during cell death. Cell Death Differ 15:1857–1864
25. Wang Y, Kim NS, Li X, Greer PA, Koehler RC, Dawson VL, Dawson TM (2009) Calpain activation is not required for AIF translocation in Parp-1-dependent cell death (Parthanatos). J Neurochem 110:687–696
26. Morishima N, Nakanishi K, Takenouchi H, Shibata T, Yasuhiko Y (2002) An endoplasmic reticulum stress-specific caspase cascade in apoptosis. Cytochrome c-independent activation of caspase-9 by caspase-12. J Biol Chem 277:34287–34294
27. Nakagawa T, Zhu H, Morishima N, Li E, Xu J, Yankner BA, Yuan J (2000) Caspase-12 mediates endoplasmic-reticulum-specific apoptosis and cytotoxicity by amyloid-beta. Nature 403:98–103
28. Szegezdi E, Logue SE, Gorman AM, Samali A (2006) Mediators of endoplasmic reticulum stress-induced apoptosis. EMBO Rep 7:880–885
29. Bari MR, Akbar S, Eweida M, Kuhn FJ, Gustafsson AJ, Luckhoff A, Islam MS (2009) H_2O_2-induced Ca^{2+} influx and its inhibition by *N*-(*p*-amylcinnamoyl)anthranilic acid in the beta-cells: involvement of TRPM2 channels. J Cell Mol Med 13:3260–3267

30. Kraft R, Grimm C, Frenzel H, Harteneck C (2006) Inhibition of TRPM2 cation channels by *N*-(*p*-amylcinnamoyl)anthranilic acid. Br J Pharmacol 148:264–273
31. Pantaler E, Luckhoff A (2009) Inhibitors of TRP channels reveal stimulus-dependent differential activation of Ca^{2+} influx pathways in human neutrophil granulocytes. Naunyn Schmiedebergs Arch Pharmacol 360:497–507
32. Orrenius S, Gogvadze V, Zhivotovsky B (2007) Mitochondrial oxidative stress: implications for cell death. Annu Rev Pharmacol Toxicol 47:143–183
33. Ame JC, Rolli V, Schreiber V, Niedergang C, Apiou F, Decker P, Muller S, Hoger T, Menissier-de Murcia J, de Murcia G (1999) PARP-2, a novel mammalian DNA damage-dependent poly (ADP-ribose) polymerase. J Biol Chem 274:17860–17868
34. Ame JC, Schreiber V, Fraulob V, Dolle P, de Murcia G, Niedergang CP (2001) A bidirectional promoter connects the poly(ADP-ribose) polymerase 2 (PARP-2) gene to the gene for RNase P RNA. Structure and expression of the mouse PARP-2 gene. J Biol Chem 276:11092–11099
35. Schreiber V, Ame JC, Dolle P, Schultz I, Rinaldi B, Fraulob V, Menissier-de Murcia J, de Murcia G (2002) Poly(ADP-ribose) polymerase-2 (PARP-2) is required for efficient base excision DNA repair in association with PARP-1 and XRCC1. J Biol Chem 277:23028–23036
36. Althaus FR, Richter C (1987) ADP-ribosylation of proteins. Enzymology and biological significance. Mol Biol Biochem Biophys 37:1–237
37. Sallmann FR, Vodenicharov MD, Wang ZQ, Poirier GG (2000) Characterization of sPARP-1. An alternative product of PARP-1 gene with poly(ADP-ribose) polymerase activity independent of DNA strand breaks. J Biol Chem 275:15504–15511
38. Shieh WM, Ame JC, Wilson MV, Wang ZQ, Koh DW, Jacobson MK, Jacobson EL (1998) Poly(ADP-ribose) polymerase null mouse cells synthesize ADP-ribose polymers. J Biol Chem 273:30069–30072
39. Buelow B, Uzunparmak B, Paddock M, Scharenberg AM (2009) Structure/function analysis of PARP-1 in oxidative and nitrosative stress-induced monomeric ADPR formation. PLoS One 4:e6339. doi:10.1371/journal.pone.0006339
40. Perraud AL, Fleig A, Dunn CA, Bagley LA, Launay P, Schmitz C, Stokes AJ, Zhu Q, Bessman MJ, Penner R, Kinet JP, Scharenberg AM (2001) ADP-ribose gating of the calcium-permeable LTRPC2 channel revealed by Nudix motif homology. Nature 411:595–599
41. Wehage E, Eisfeld J, Heiner I, Jungling E, Zitt C, Luckhoff A (2002) Activation of the cation channel long transient receptor potential channel 2 (LTRPC2) by hydrogen peroxide. A splice variant reveals a mode of activation independent of ADP-ribose. J Biol Chem 277:23150–23156
42. Gasser A, Glassmeier G, Fliegert R, Langhorst MF, Meinke S, Hein D, Kruger S, Weber K, Heiner I, Oppenheimer N, Schwarz JR, Guse AH (2006) Activation of T cell calcium influx by the second messenger ADP-ribose. J Biol Chem 281:2489–2496
43. Gasser A, Guse AH (2005) Determination of intracellular concentrations of the TRPM2 agonist ADP-ribose by reversed-phase HPLC. J Chromatogr B Analyt Technol Biomed Life Sci 821:181–187
44. Hansen KB, Brauner-Osborne H (2009) FLIPR assays of intracellular calcium in GPCR drug discovery. Methods Mol Biol 552:269–278
45. Klonowski-Stumpe H, Schreiber R, Grolik M, Schulz HU, Haussinger D, Niederau C (1997) Effect of oxidative stress on cellular functions and cytosolic free calcium of rat pancreatic acinar cells. Am J Physiol 272:G1489–G1498
46. Kilpatrick LE, Jakabovics E, McCawley LJ, Kane LH, Korchak HM (1995) Cromolyn inhibits assembly of the NADPH oxidase and superoxide anion generation by human neutrophils. J Immunol 154:3429–3436
47. Sato H, Takeo T, Liu Q, Nakano K, Osanai T, Suga S, Wakui M, Wu J (2009) Hydrogen peroxide mobilizes Ca^{2+} through two distinct mechanisms in rat hepatocytes. Acta Pharmacol Sin 30:78–89
48. Burns DM, Ying W, Kauppinen TM, Zhu K, Swanson RA (2009) Selective down-regulation of nuclear poly(ADP-ribose) glycohydrolase. PLoS One 4:e4896
49. Erdelyi K, Bai P, Kovacs I, Szabo E, Mocsar G, Kakuk A, Szabo C, Gergely P, Virag L (2009) Dual role of poly(ADP-ribose) glycohydrolase in the regulation of cell death in oxidatively stressed A549 cells. Faseb J 23:3553–3563
50. Formentini L, Arapistas P, Pittelli M, Jacomelli M, Pitozzi V, Menichetti S, Romani A, Giovannelli L, Moroni F, Chiarugi A (2008) Mono-galloyl glucose derivatives are potent poly(ADP-ribose) glycohydrolase (PARG) inhibitors and partially reduce PARP-1-dependent cell death. Br J Pharmacol 155:1235–1249
51. Zhang W, Hirschler-Laszkiewicz I, Tong Q, Conrad K, Sun SC, Penn L, Barber DL, Stahl R, Carey DJ, Cheung JY, Miller BA (2006) TRPM2 is an ion channel that modulates hematopoietic cell death through activation of caspases and PARP cleavage. Am J Physiol Cell Physiol 290:C1146–C1159
52. Yamamoto S, Shimizu S, Kiyonaka S, Takahashi N, Wajima T, Hara Y, Negoro T, Hiroi T, Kiuchi Y, Okada T, Kaneko S, Lange I, Fleig A, Penner R, Nishi M, Takeshima H, Mori Y (2008) TRPM2-mediated Ca^{2+} influx induces chemokine production in monocytes that aggravates inflammatory neutrophil infiltration. Nat Med 14:738–747
53. Naziroglu M, Luckhoff A (2008) A calcium influx pathway regulated separately by oxidative stress and ADP-Ribose in TRPM2 channels: single channel events. Neurochem Res 33:1256–1262
54. Kuhn FJ, Luckhoff A (2004) Sites of the NUDT9-H domain critical for ADP-ribose activation of the cation channel TRPM2. J Biol Chem 279:46431–46437
55. Formentini L, Macchiarulo A, Cipriani G, Camaioni E, Rapizzi E, Pellicciari R, Moroni F, Chiarugi A (2009) Poly(ADP-ribose) catabolism triggers AMP-dependent mitochondrial energy failure. J Biol Chem 284:17668–17676
56. Hecquet CM, Malik AB (2009) Role of H_2O_2-activated TRPM2 calcium channel in oxidant-induced endothelial injury. Thromb Haemost 101:619–625
57. Tang JB, Goellner EM, Wang XH, Trivedi RN, St Croix CM, Jelezcova E, Svilar D, Brown AR, Sobol RW (2010) Bioenergetic metabolites regulate base excision repair-dependent cell death in response to DNA damage. Mol Cancer Res 8:67–79